Crystallography of ultrathin iron, cobalt and nickel films grown epitaxially on copper

1999 J. Phys.: Condens. Matter 11 9437

(http://iopscience.iop.org/0953-8984/11/48/307)

J. Phys.: Condens. Matter **11** (1999) 9437–9454. Printed in the UK PII: S0953-8984(99)06475-9

Crystallography of ultrathin iron, cobalt and nickel films grown epitaxially on copper

K Heinz†, S Müller‡ and L Hammer

Universität Erlangen–Nürnberg, Lehrstuhl für Festkörperphysik, Staudtstrasse 7, D-91058 Erlangen, Germany

E-mail: kheinz@fkp.physik.uni-erlangen.de

Received 30 July 1999

Abstract. Though correlations between surface structure and magnetism are evident, surface structure determinations of ultrathin magnetic films in the crystallographic sense are available only for a few cases. We investigate the three examples Ni/Cu(100), Co/Cu(111) and Fe/Cu(100) which each exhibit only little film–substrate lattice misfit but which are rather different as regards the native lattice symmetry of the materials involved. Correspondingly, the structures of the films are rather different. They are described for various film thicknesses in each case and a comparison with the magnetic properties is made.

1. Crystallographic degrees of freedom for hetero-epitaxial pseudomorphic growth

As is well known, the hetero-epitaxial growth of a material on a certain surface of a crystalline substrate can be pseudomorphic when the lattice parameters involved are not too different. More precisely, as two surface orientations of the two materials need to match, there must be a certain surface orientation of the growing film whose lateral lattice parameter is close to that of the substrate surface chosen. In a simple picture it is frequently assumed that the film just continues the substrate lattice in a nearly undistorted way, with the result that a new material with the ideal substrate lattice should develop. Obviously, in this case the film would not be very interesting from the crystallographic point of view and it might be for that reason that it took some time for quantitative crystallographic analyses of epitaxial pseudomorphic films to get started.

However, things are of course not as simple as described above. Even when the native film and substrate material have the same type of lattice, the lattice parameters may not exactly fit, i.e. the film can be laterally either compressed or expanded compared to the native form of the growing material. With pseudomorphic layer-by-layer growth (if this takes place) proceeding, the film 'realizes' that there is lateral misfit because of the energy cost involved. This is in principle already happening during the formation of the second epitaxial layer, and the film tries to compensate for it by perpendicular (vertical) distortion. The simplest case to think of in this respect is some tetragonal distortion in an appropriate direction to preserve the atomic volume, i.e. vertical layer spacings compared to those of the native bulk material are being modified accordingly. Of course, there is still some energy cost for the overall distortion and

† Author to whom any correspondence should be addressed.
‡ Present address: National Renewable Energy Laboratory, Golden, CO, USA.

0953-8984/99/489437+18$30.00

the film must be expected to transform to the geometry of the native material when a critical thickness, i.e. energy cost, is reached. This still rather simple scenario holds for the growth of e.g. Ni on Cu(100) and we will focus on this case in the second section.

If the lattice types of the native film material and the substrate are different, the situation can become more complex, though this is not necessarily the case. For example, by the pseudomorphic growth of Co on Cu(100), rather thick and almost ideal fcc-Co films can be formed. This is because the interatomic distances in Cu and native hcp-Co are very close and the total-energy difference between hcp- and fcc-Co is rather small, so the distortion energy due to the lateral expansion and the 'wrong' crystallographic structure is small, too. For the growth of Co on Cu(111), however, growing Co layers have the freedom to stack either in an fcc sequence (so continuing the substrate) or in the native hcp sequence, which at room temperature is (slightly) favoured energetically for bulk cobalt. This opens up the possibility for a gradual transformation from fcc to hcp structure which in fact takes place, as will be discussed in section 3. We also include the issue of sandwich structures, i.e. the structure of the film when capped by additional copper layers, either floated to the surface from the substrate or intentionally deposited.

Even when there is no freedom to change the layer stacking sequence, e.g. for the growth of native bcc-type material on an fcc(100) substrate, rather complex structures can develop. For example, on deposition of Fe on Cu(100) the resulting Fe films turn out to be heavily reconstructed, exhibiting atomic displacements from the ideal fcc positions, so the film may be considered to be fcc only on average. We investigate this case in section 4, including the film's transition back to bcc structure when a certain critical thickness is reached.

As in the present paper the focus is on the crystallography of ultrathin magnetic films, it is obvious that we must concentrate on rather well defined cases, e.g. cases where pseudomorphic layer-by-layer growth is observed or at least large film domains with well defined structure in the crystallographic sense exist. As this is rather restrictive (see e.g. the contribution of E Bauer in this Special Issue) and as quantitative structure determination is rather demanding, at least in the case of non-trivial structures, not many such crystallographic analyses are available. As our own work covers the above-described different and rather typical cases of crystallographically well defined magnetic thin films, we concentrate on these in the present paper. Quantitative low-energy electron diffraction (LEED) was applied as the structural probe. As there are a number of methodical reviews of the technique available (see e.g. reference [1] for a recent review and references therein), we avoid giving details of the analysis in each case and focus on the structural results obtained. A comparison of the latter to the magnetic properties of the films is made in order to detect possible correlations between structure and magnetism.

2. Structural simplicity versus magnetic complexity: ultrathin Ni films on Cu(100)

The lattices of nickel and copper are both of fcc type and their interatomic distances differ only by 2.5% (bulk values at room temperature: 2.49 Å and 2.56 Å, respectively). Not surprisingly therefore, well defined pseudomorphic growth up to more than ten monolayers (ML) has been observed for the deposition of nickel on Cu(100) and a number of investigations concerning the electronic and magnetic properties of the films have been carried out (see also the contribution of P Poulopoulos and K Baberschke in this Special Issue or reference [2]). In view of the lateral expansion of the nickel films imposed by pseudomorphic growth ($\epsilon_1 = 2.5\%$), the film should be distorted tetragonally, whereby from the elastic properties of bulk nickel described by the elastic constants c_{12} and c_{11} a value of $\epsilon_2 \approx -2c_{12}\epsilon_1/c_{11} = -3.2\%$ results. Using the magnetostriction constant for bulk nickel, $\lambda_{100} = -5.5 \times 10^{-7}$ [3], the magnetic uniaxial

volume anisotropy constant for a thick film turns out to be

$$K_V = \frac{3}{2}\lambda_{100}(c_{11} - c_{12})(\epsilon_2 - \epsilon_1) = 29\ \mu\text{eV/atom}.$$

This value is larger by three orders of magnitude than the corresponding value for an undistorted nickel crystal (and additionally differs in sign). It has been experimentally confirmed quantitatively ($K_V = 30\ \mu$eV/atom [4]). Therefore, it is interesting to find out whether the underlying tetragonal distortion of the order of -3% can be confirmed quantitatively, too. In particular, it will be of interest to establish whether or not the tetragonal distortion of the film is uniform, thickness and/or temperature dependent etc. This is particularly important also in view of the rather complex magnetic film properties which are characterized by the findings that the Curie temperature of the film is thickness dependent (e.g. $T_C = 225$ K for 4 ML) and that in the ferromagnetic regime the film magnetization switches from being in the plane for very low coverages to normal to the surface at a critical film thickness ($d_C = 7$ ML at 200 K). The question arises of whether these magnetic transitions, ferromagnetic to paramagnetic or from in-plane to perpendicular (vertical) magnetization, are accompanied by detectable structural modifications. As the latter can develop via changes of nickel interlayer spacings only (due to the pseudomorphic growth), analyses of the multilayer relaxation of the films as a function of temperature and film thickness are desirable. Fortunately, quantitative LEED is very sensitive to vertical parameters, so it is the appropriate method for approaching the problem described. Yet, as the magnetic order–disorder transition or the magnetic reorientation might have only little effect on the film structure (see below), high accuracy is demanded for the structure analyses. In particular, residual gas adsorption should be avoided, as it is known to modify the multilayer relaxation, which is why earlier measurements [5] had to be repeated [6].

A sequence of films of different thicknesses (1, 2, 3, 4, 5, 7, 11 ML) in the range covering the reorientation from in-plane to perpendicular (vertical) magnetization were prepared; using these, layer-by-layer growth was checked and monitored via medium-energy electron diffraction (MEED) oscillations [6]. For each coverage the films were annealed at about 400 K in order to produce smooth surfaces, a procedure which has been proved to be successful by scanning tunnelling microscopy [7]. LEED intensity spectra, $I(E)$, were collected at normal incidence of the primary beam using a computer-controlled and video-based technique [8, 9]. For the 4 ML and 7 ML films, measurements at temperatures below and above the Curie temperature were performed. Intensities were measured for electron energies up to 600 eV, providing a broad database (typically an accumulated total of 2000 eV for a set of spectra for each temperature and coverage). So high structural accuracy is possible and simultaneously there is access also to deep-lying interlayer spacings in the case of thicker films. Excellent comparison between experimental data and spectra calculated according to the best-fit model could be achieved in each case, i.e. both for different film thicknesses and for different temperatures. This is expressed by the Pendry R-factors [10] being of the order of only $R_P = 0.1$. With the total-energy width of the database of about 2000 eV, in most cases errors for the interlayer spacings were in the range 0.01–0.02 Å depending on the layer depth.

Table 1 displays in the first column the interlayer spacings of a 7 ML nickel film that is ferromagnetic at the temperature of measurement (80 K) with the magnetization being in the plane. We note that all spacings are in a rather narrow range around 1.70 Å. Compared to the case for undistorted nickel ($d_{i,i+1} = 1.76$ Å), this corresponds to a tetragonal distortion of -3.4% which is practically identical to the value calculated from the simple elastic deformation considerations above (compared to the pseudomorphic, i.e. expanded, surface unit mesh, the distortion is -5.6%). As all spacings coincide within the limits of error, we can conclude that the tetragonal distortion is homogeneous throughout the film. In turn, this *a posteriori* justifies the approach described above for calculating the anisotropy coefficient and makes the almost

Table 1. Spacings $d_{i,i+1}$ between the ith and $(i + 1)$th layers in a 7 ML nickel film grown epitaxially on Cu(100). The left-hand column corresponds to a temperature (80 K) for which the film magnetization is in the plane and the right-hand column to one (300 K) for which the magnetization is normal to the surface. The quantity d_b corresponds to the (weighted-) average spacing below the sixth nickel layer and R denotes the best-fit Pendry R-factor (after reference [6]).

Parameter	80 K	300 K
d_{12} (Å)	1.710 ± 0.011	1.685 ± 0.016
d_{23} (Å)	1.695 ± 0.011	1.705 ± 0.018
d_{34} (Å)	1.695 ± 0.010	1.690 ± 0.019
d_{45} (Å)	1.700 ± 0.015	1.710 ± 0.025
d_{56} (Å)	1.710 ± 0.022	1.70 ± 0.06
d_b (Å)	1.70	1.70
R	0.111	0.112

identical experimental value appear either as no surprise or as an impressive confirmation of the applicability of the above simple considerations.

The features described hold also for other film thicknesses, for which the same degree of tetragonal distortion is detected. So, the films are homogeneously distorted tetragonally and also independently of the film thickness. In particular, within the limits of error achieved there is no structural change upon the easy magnetic axis switching from being in the plane to perpendicular to the surface. This is clearly apparent from the right-hand column of table 1: at the temperature given (300 K), the film magnetization is normal to the surface (transition range: 200–260 K) and still practically the same structural parameter values apply. The same is true for the magnetic order–disorder transition as a function of temperature, as has been shown in great detail for a 4 ML film with a Curie temperature of 225 K [6]. The reader should note that the thermal expansion in the temperature range under consideration is negligible, i.e. less than 0.002 Å per layer spacing.

So, the dominant structural feature of ultrathin nickel films on Cu(100) is their spatially homogeneous and thickness-independent tetragonal distortion. The degree of the latter is largely determined by the requirement of preserving the atomic volume, which is 10.92 Å^3 for bulk nickel and 10.88 Å^3 for the films. Any magnetostriction effects caused by magnetic transitions, i.e. by changes of the magnetic order or of the easy magnetic axis, are below the limit of detection for surface structure determination (0.01 Å). This means that—contrary to earlier speculations—magnetostriction effects at the surface are not very strongly enhanced and are in fact probably of similar magnitude to those in the bulk (0.0001 Å). This is supported by first-principles calculations [11].

3. Interface-dictated layer stacking: Co films on Cu(111) and Cu/Co/Cu sandwiches

From the lattice misfit point of view, the growth of Co on Cu is similarly favourable to that of the Ni–Cu system: the interatomic distances in Cu and Co bulk differ by only 2% ($a_{\mathrm{Co}} = 2.505$ Å). At first glance, this leads to the expectation that pseudomorphic growth of the two metals one on top of the other should exhibit nothing spectacular and indeed this is rather true for the growth in the (100) orientation [12]. On the (111) surface, however, the growing material has the freedom to stack in an fcc or hcp sequence. This is of particular importance for the growth of Co/Cu(111) superlattices with cobalt layers stacked in an fcc sequence. These superlattices exhibit strong magnetic anisotropy with oscillatory magnetic coupling (OMC) across the non-magnetic layers and an associated giant magnetic resistance (GMR) which, however, is reduced

when the Co/Cu interface is rough and/or stacking faults develop in the cobalt film [13]. For ultrathin Co films on Cu(111), perpendicular magnetic anisotropy has been found [14].

A number of studies have been performed with the aim of finding the structure and, in particular, the stacking of cobalt layers on Cu(111), wherein various methods, e.g. visual [15–17] and quantitative [18–21] LEED, angle-resolved photoelectron scattering [16, 17, 22, 23], Auger electron forward scattering [17], scanning tunnelling microscopy (STM) [21, 24–26], thermal energy atom scattering [18], low-energy ion scattering [27], angle-resolved secondary-electron back scattering [28] and extended x-ray absorption fine-structure (EXAFS) measurements [29, 30], were applied. Structural information about Co/Cu(111) superlattices was obtained by nuclear magnetic resonance (NMR) experiments [31–34] and x-ray diffraction [33–36]. Detailed information was supplied recently by quantitative LEED combined *in situ* with STM investigations [18–21]. LEED is extremely sensitive to both interlayer spacings and the stacking character of layers, as has been demonstrated explicitly for the Co/Cu(111) system [37]. Yet, whilst the stacking can be established down to the sixth layer in the surface, discrimination between cobalt and copper is reliably possible only for the first two layers because of the similar scattering properties of the two elements [19–21]. As it turns out that the growth of Co on Cu(111) depends sensitively on whether or not the growing film is capped by copper layer(s), either intentionally or as a result of them floating up from the substrate, it is worthwhile to present the two cases separately.

3.1. Co films on Cu(111): from fcc to hcp stacking

Pure fcc stacking (as in Cu(111)) or pure hcp stacking (as in Co(0001)) is immediately apparent from the symmetry of the respective LEED patterns. Whilst at normal incidence of the primary beam the diffraction pattern is threefold symmetric for fcc(111) surfaces, surface steps make it always effectively sixfold symmetric for hcp(0001) surfaces. Therefore, the (10) and (01) beam spectra are equivalent for hcp, but completely different for fcc surfaces. As a consequence, by simply recording these two beam spectra for the growth of Co on Cu(111), some key information about the evolution of the layer stacking can already be gained without the demanding dynamical interpretation of the data that is usually necessary.

Figure 1 displays the result of such a measurement for cobalt coverages up to above 5 ML. Apparently, up to coverages of 2 ML the cobalt film largely copies the fcc stacking of the substrate. Above this coverage, the (10) and (01) beam spectra become more and more similar, i.e. the growing film is increasingly dominated by hcp stacking. So, there is a gradual transition of the film from fcc to hcp as predicted much earlier theoretically [38, 39]. Around and above 5 ML coverage, the spectra almost coincide. Also, they are in very close agreement with data taken from the (0001) surface of a Co bulk crystal, proving the dominance of hcp stacking in the film. Consistently, the spectra are very different to data resulting from a calculated superposition of equally weighted domains of twinned fcc domains (see the top spectrum in figure 1), which would also produce an effectively sixfold-symmetric diffraction pattern.

Of course, the above interpretation of the data reflects only some lateral average of the film growth. STM investigations carried out in parallel indicate that the growth is three dimensional rather than layer by layer [24, 25], i.e. islands of different size and height must be considered. Therefore, a more detailed and quantitative analysis of the LEED intensity spectra (including all accessible beams) must allow for several domains of different film thicknesses, of different stacking sequences and of different chemistry. The latter is advisable in view of the fact that for very thin films copper atoms cap part of the cobalt film, as confirmed by a number of investigations and methods such as photoelectron diffraction [16, 17], low-energy

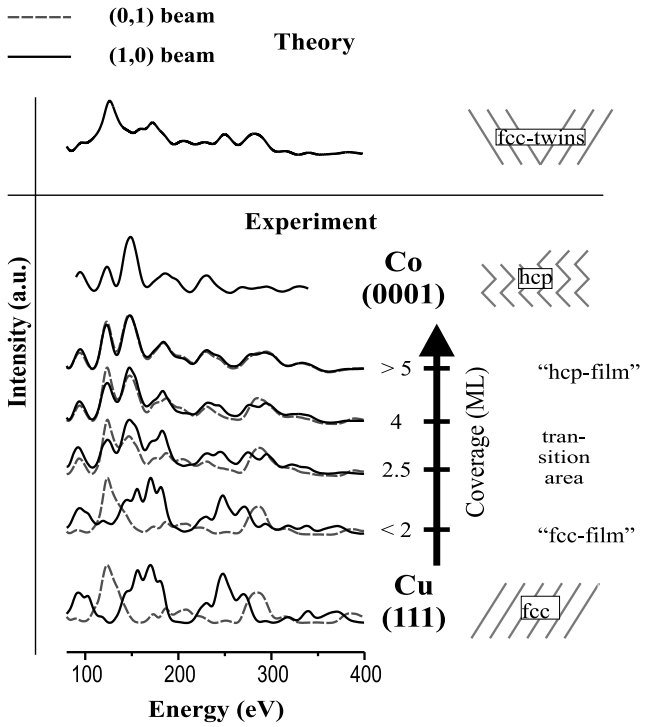

Figure 1. In the bottom panel, experimental LEED spectra of the (10) and (01) beams for clean Cu(111) and Co(0001) and for various coverages of Co on Cu(111) are displayed. The spectrum in the top panel was calculated for an artificial cobalt film grown fully fcc, but exhibiting twins and so simulating sixfold symmetry.

ion scattering [22, 27], STM using CO titration [26] and quantitative LEED [20]. The Cu capping is favoured by the considerably lower surface free energy of copper (1.934 J m^{-2}) compared to that of cobalt (2.709 J m^{-2}). Moreover, recent time-resolved STM work, together with *ab initio* calculations, has revealed that Cu atoms are etched from the top substrate layer by a Co–Cu substitution process, with the result that eventually Cu–Co–Co trilayers are formed which are (partly) incorporated in the substrate [40]. The LEED analysis of a cobalt film (nominally) 1.5 ML thick is in nice agreement with these findings, as is obvious from the upper panel in figure 2 which schematically displays the domain distribution according to the best-fit achieved (Pendry R-factor: $R = 0.12$) [21]. There are always bilayers of Co with some 25% of the surface still uncovered. In a large copper-capped domain, 45% of the surface cobalt has substituted for Cu atoms of the top substrate layer. Although this latter finding is not outside the limits of error (due to the above-mentioned similarity of the scattering characteristics of cobalt and copper atoms), it corresponds to the best fit achieved and it is highly probable also since it reproduces the correct total coverage (1.5 ML), as independently determined by AES. Small patches of the cobalt double layers are not capped by copper. They show either fcc or hcp stacking, the latter indicating that stacking faults (with respect to the stacking given by the substrate) are already developing at rather low coverages. These stacking faults increase in number with increasing film thickness, as is evident from the lower panels in figure 2. Figure 3 shows in the top panel that at 5 ML coverage the film has almost completely adopted hcp stacking. Yet, one must keep in mind that the film growth above the first cobalt double layer

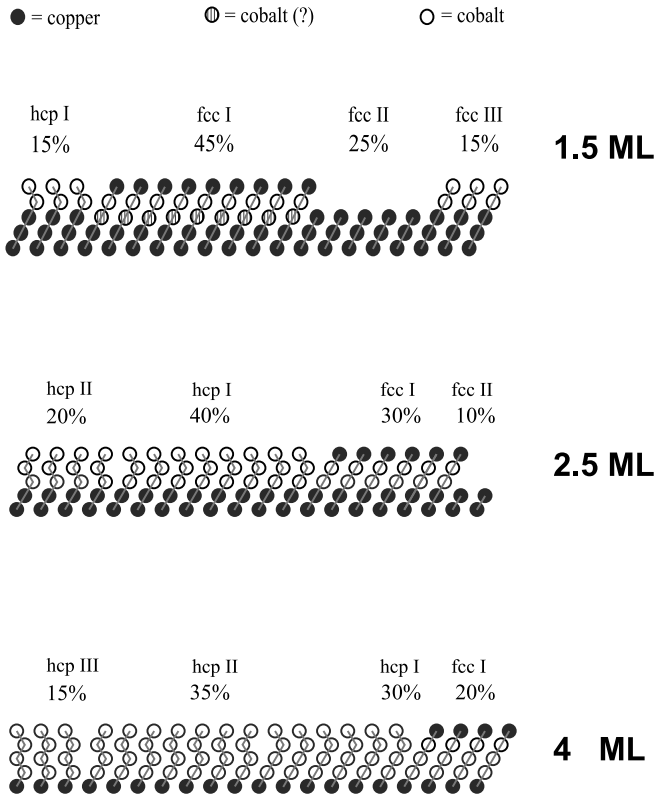

Figure 2. Domain distributions (schematic) in ultrathin Co films on Cu(111) for different Co coverages as indicated. Layers arranged linearly (in zigzags) correspond to fcc (hcp) stacking. The chemical nature of the hatched atoms could not be determined reliably.

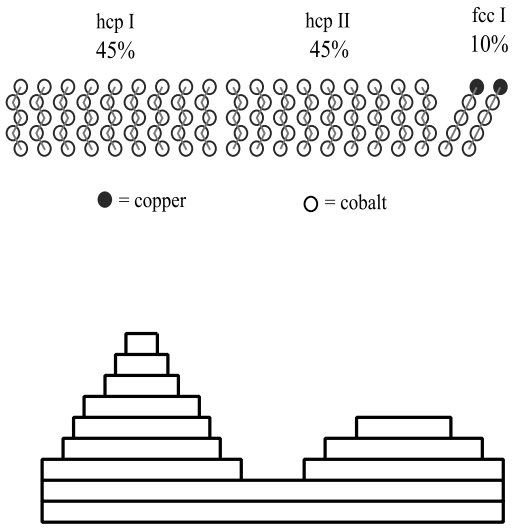

Figure 3. In the top panel the stacking sequence for a Co coverage of 5 ML is displayed. The bottom panel indicates schematically that there is a distribution of pyramid-shaped islands.

is three dimensional, as displayed schematically in the bottom panel of figure 3. STM images show that the islands are of pyramid shape with the layer population exhibiting a Poisson distribution [24, 25]. It might be because of this rather open morphology that the lateral lattice parameter of the cobalt film can relax from the copper-dictated value (2.56 Å) to the cobalt bulk value (2.51 Å), as clearly indicated by quantitative LEED analyses [21]. For all domains the interlayer distances are in agreement with the hard-core radii of cobalt and copper. For thick cobalt films almost the same (weak) multilayer relaxation is found as for the (0001) surface of a bulk cobalt crystal with the top-layer spacing contracted by about 3% [41].

It is obvious from figure 2 that Co domains capped by Cu always show fcc stacking. So, in a cobalt film sandwiched between copper layers, stabilization of fcc stacking should be expected, which is indeed what is found as will be demonstrated in more detail in the next subsection. As floating of copper to the surface becomes more and more unlikely with increasing film thickness [27], the weight of the Co domains which have switched to hcp stacking increases accordingly, as quantitatively displayed in figure 4. Yet, in the literature rather different coverages are reported at which the cobalt film has transformed to having hcp structure. However, this is not surprising, as the extent to which copper floats to the surface (either from uncovered areas or by the cobalt etching process mentioned above) must be expected to depend considerably on the preparation conditions, such as temperature, evaporation rate and time between deposition and observation. Also, the quality of the substrate in terms of step density seems to be of some importance, i.e. a high density of substrate steps seems to favour fcc stacking [21, 24] and the transition to hcp then develops only at higher coverages [19, 20].

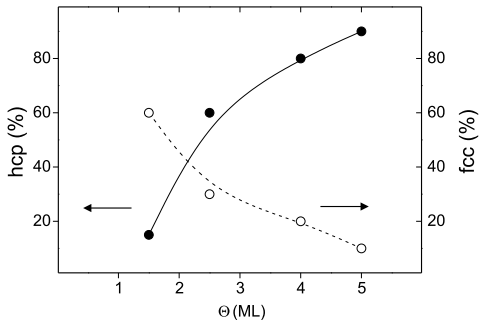

Figure 4. Percentage of surface areas covered by Co domains having adopted hcp stacking or still showing fcc stacking, both as functions of coverage Θ.

3.2. Cu/Co/Cu(111) sandwiches: stabilization of fcc stacking

For Cu/Co/Cu(111) sandwich structures it has been frequently reported that the Co layers predominantly show fcc stacking [31–36]. Though this seems to be at variance with pure cobalt films having already switched to hexagonal close packing even at rather low coverages, it is in nice agreement with the observation that in copper-capped thin-film domains fcc stacking is preserved. Seemingly, the influence of two Co–Cu interfaces dictates fcc stacking throughout the whole film; this is certainly favoured by the only small energy cost compared to that of hcp stacking (28 meV/atom [42]). To shed more light on this scenario, the structures of thin Co films additionally and intentionally covered by a few copper layers were investigated.

At very low coverages (1.5 ML), at which the film is predominantly fcc type, of course nothing dramatic happens. Fcc stacking is preserved, but twin domains are already starting to develop. The LEED pattern's symmetry is still threefold. For thicker cobalt films, e.g. 5 ML

of Co, a dramatic change takes place when the film is additionally covered by 2 ML of Cu. Although the sixfold symmetry observed for the pure film is preserved, the intensity spectra change completely, as demonstrated in the top panel of figure 5. The full dynamical analysis clearly shows [21] that equally weighted fcc twins have developed, as schematically displayed in the bottom panel of figure 5. The fcc stacking seems to hold for the full cobalt film, but is reliably detected outside the error limits only in the top five layers (including the two Cu layers).

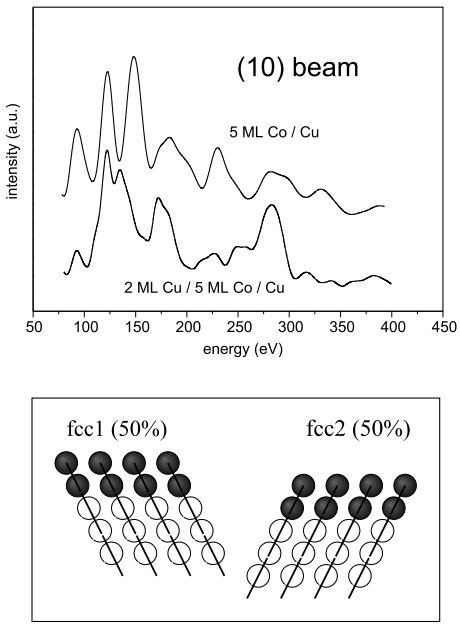

Figure 5. In the top panel, $I(E)$ spectra for the (10) beam for a 5 ML Co film on Cu(111) and for a 2 ML/5 ML Co/Cu(111) sandwich are displayed. In the bottom panel, the development of fcc twin domains is indicated.

The fcc stacking obtained is much in line with the results reported for Co/Cu superlattices, e.g. $\{5\text{ ML Co}/3\text{ ML Cu}\}_{111}$ grown at room temperature [33], i.e. very close to our present preparation and layer sequence conditions. Yet, it is rather surprising in view of the hcp stacking of the uncovered 5 ML Co film on which the additional 2 ML of Cu were deposited. We remind the reader that no or only a negligible amount of copper has floated to the top of this film. This might happen during growth at elevated temperatures, and fcc stacking in so-prepared superlattices [34, 36] might be stabilized by Cu steadily floating to the surface. Also, a kind of 'surface pump mechanism' has been reported recently [43]. According to this, metastable Co–Cu alloys are formed at elevated temperatures with subsequent decomposition, whilst at lower temperatures Cu is reported to find its way to the surface through pinholes. In the present case, however, the situation is more complicated, as at least the total top layer of the cobalt film must have changed its stacking from hcp to fcc upon deposition of the Cu layers. This requires the lateral movement of a full layer and so cannot easily be explained by some adsorbate-induced (here Cu-induced) reconstruction, as this is usually only local (however, in some cases extended surface modifications such as a missing-row reconstruction also take place [44]). Also, it has been reported for the growth of Au on Ni(111) that partial-misfit dislocation loops can be induced in the substrate [45]. Upon formation of vacancies within

the substrate, nickel atoms shift from fcc to hcp sites, as a result of which a finite-sized and triangle-shaped loop is formed. Though this modification of the substrate is rather drastic, only a few atoms are induced to move, whilst in the present case all top-layer atoms of a domain are involved. Yet, one should again remember that the cobalt film grows in islands, i.e. the layers are of finite extent. This, by some still unresolved process, might allow for the stacking rearrangement detected, possibly also involving deeper cobalt layers.

4. Growth of Fe on Cu(100): unexpected structural complexity

The growth of Fe on Cu(100) at room temperature or below allows the stabilization of fcc-iron (γ-Fe), which is normally stable only in the higher-temperature regime (1185 K $< T <$ 1667 K). Theoretical investigations show that as the lattice parameter varies there are a variety of magnetic states [46, 47], in particular non-magnetic, ferromagnetic high- and low-spin and antiferromagnetic phases of fcc-Fe, which are seemingly close energetically. This is in agreement with the Invar effect observed rather early in alloys and interpreted in terms of the existence of distinct configurations of fcc-iron [48]. So, e.g. for an atomic volume $V_a = 12.05$ Å^3, fcc-Fe should be ferromagnetic whilst it should be antiferromagnetic for $V_a = 11.4$ Å^3. This makes Cu(100) a very interesting substrate for the stabilization of fcc-Fe films, as ideal undistorted growth would lead to a volume of $V_a = 11.76$ Å^3, so only slight tetragonal distortions in the film should lead to one or other of the magnetic phases as predicted theoretically, in fact [49–51]. Not surprisingly therefore, the epitaxial growth of fcc-Fe on Cu(100) has attracted much attention for more than a decade and even today Fe/Cu(100) is considered as 'the single most complex and complicated ultrathin magnetic system of all' [50]. Both structural and magnetic properties of such films have been studied extensively (see e.g. references [17, 52–99]); in most cases the films were deposited thermally. A few investigations using pulsed laser deposition have been carried out, too (see e.g. references [100, 101]). For investigations of the magnetic properties, in most cases the surface magneto-optical Kerr effect (SMOKE) or magnetization-induced second-harmonic generation (MSHG) was applied, with access to the crystallographic structure provided by x-ray absorption fine-structure measurements and, dominantly, by quantitative LEED.

Figure 6 [94] presents an overview on the obviously strong correlation between magnetic and structural properties as a function of film thickness, as appearing through the SMOKE remanence signal and the LEED patterns, respectively. With iron deposition on the substrate at room temperature, the magnetic signal with the magnetic anisotropy perpendicular to the surface increases with coverage up to about 4 ML [69], indicating that the film is ferromagnetic throughout its entire volume. In this coverage regime, strong surface reconstructions of 4×1 and 5×1 periodicities are observed which, however, must be of special structure, as extra spots appear only as satellites of the substrate spots [86]. We will see below that in these films all layers are reconstructed, i.e. the number of reconstructed layers increases with film thickness in accordance with the thickness-dependent remanence signal. Near and above 4 ML coverage, the magnetic signal strongly decreases and it remains independent of coverage up to about 10–11 ML. In this regime, in which the magnetization is still perpendicular to the surface, a 2×1 superstructure with $p2mg$ symmetry is observed, fading away, however, with increasing coverage. As will be shown below, the thickness-independent magnetic signal in this regime is in agreement with only the top layer of the films being reconstructed, whereby the reconstruction loses long-range order with increasing coverage but is preserved locally. At around 10 ML the film magnetization starts to switch from perpendicular to parallel to the surface, which is indicative of the film's transition to bcc structure, i.e. to the native structure of iron at room temperature. This is consistent with the development of a new 'superstructure' in

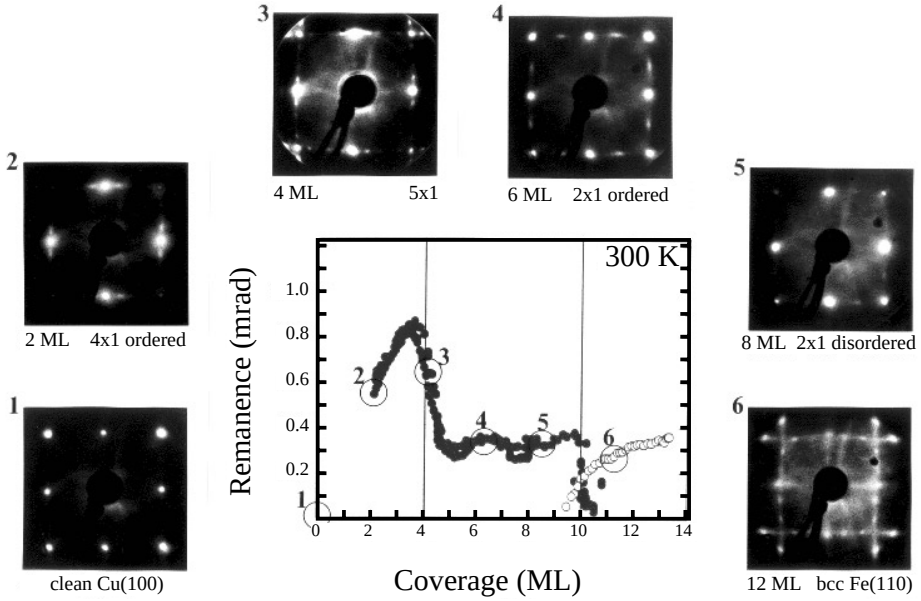

Figure 6. A survey of the structural and magnetic properties of ultrathin Fe films on Cu(100) as a function of the coverage (after reference [94]).

the diffraction pattern, which was originally labelled '3×1' [63, 72] but from a more detailed investigation turns out to be due to a bcc-iron Fe(110) film arranged in domains of different orientations on the fcc(100) substrate [85]. When iron is deposited at 100 K, the transition to bcc is already near a coverage of 5 ML [86]. On the other hand, the transition can be shifted to much higher coverages when e.g. CO is adsorbed on the surface [93].

In view of the number and complexity of the structures involved, we describe them in two separate subsections.

4.1. Ferromagnetic and reconstructed phases in the coverage regime up to 4 ML

Little is known about the very early phases of Fe/Cu(100) growth, i.e. for coverages below 1 ML. STM investigations [74,75] and LEED spot profile analyses [80] show that there is island growth whereby the size (number) of the islands increases (decreases) with increasing coverage and/or annealing temperature. The growth mode for larger coverages has been controversial; i.e. layer-by-layer, bilayer and island growth have been reported for films grown at about 300 K [59, 65, 72, 74, 76, 84]. It appears that deposition far below room temperature produces rough films which, however, become rather smooth upon room temperature annealing, without intermixing of the two elements [59, 76]. In this way, at a coverage of 2 ML a 4×1 superstructure develops (see figure 6) which gradually transforms into a 5×1 phase when the coverage approaches 4 ML. Quantitative LEED analyses of these structures show that in both phases the whole film is reconstructed, i.e. the iron atoms of all layers are displaced from the ideal fcc positions both perpendicularly (vertically) and in-plane, so the films are fcc only on average [86,87,90]. There is no indication of intermixing of atoms [9], as checked by chemical TensorLEED [102]. The structures obtained are displayed schematically in figure 7. The in-plane displacements are sinusoidal, which accounts for the fact that superstructure spots appear only as satellites of the substrate spots [60]. Both the in-plane and vertical displacements are

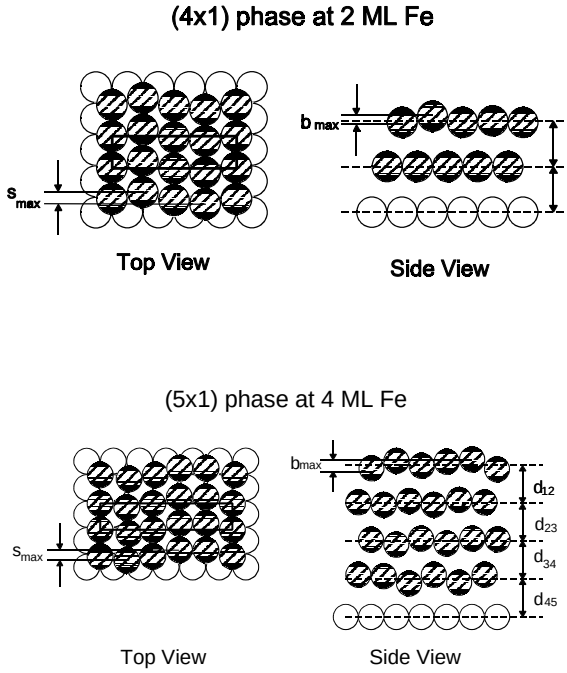

Figure 7. Structural models for the 2 ML and 4 ML phases of Fe/Cu(100) with iron atoms appearing as hatched spheres and copper atoms as white spheres (only top Fe layers are shown in the top views). The values determined for the parameters given are $d_{12} = 1.87$ Å, $d_{23} = 1.84$ Å, $b_{max} = 0.18$ Å, $s_{max} = 0.5$ Å for the 2 ML phase (i.e. the 4×1 reconstruction) and $d_{12} = 1.86$ Å, $d_{23} = 1.90$ Å, $d_{34} = 1.85$ Å, $d_{45} = 1.78$ Å, $b_{max} = 0.18$ Å, $s_{max} = 0.5$ Å for the 4 ML phase (i.e. the 5×1 reconstruction).

substantial, with maximum values (see figure 7) of $s_{max} = 0.5$ Å and $b_{max} = 0.18$ Å for the 4×1 phase and $s_{max} = 0.4$ Å and $b_{max} = 0.28$ Å for the 5×1 phase (for more structural details, see references [86, 87, 90]). As a consequence of these displacements, the interlayer spacings in the iron film are considerably enlarged compared to the spacing extrapolated from the stable high-temperature phase of fcc-Fe ($d_0 = 1.78$ Å). The average expansion of the spacings between iron layers is 5%. Equivalently, the volume occupied by an iron atom in either reconstructed phase is 12.1 Å^3, in full agreement with the above-mentioned theoretical predictions for the atomic volume necessary for ferromagnetism and in agreement with the corresponding experimental finding.

More detailed theoretical investigations were carried out recently in an attempt to describe the thickness dependency of the magnetic phases including tetragonal distortions, i.e. interlayer relaxations. The Fe/Cu interface and the interface of the Fe film with vacuum were implicitly considered in corresponding slab calculations [51]. Indeed, the films were found to be ferromagnetic up to 3 ML with an increased atomic volume of about 12.1–12.2 Å^3, i.e. very close to the experimental value. Beyond 3 ML coverage, antiferromagnetic mixed-spin states exhibit the lowest energy. Yet, due to the film's tetragonal distortion, the energy cost for a fully ferromagnetic phase at 4 ML (as observed experimentally) is only 7 meV/atom. Also, the calculations could take into consideration neither the perpendicular (vertical) buckling of layers nor their in-plane atomic shifts, due to the huge computational demands involved [51]. In view of the drastic film reconstruction, this is a considerable drawback of the calculations

(yet, computations including the reconstructions seem to be under way [51]). On the other hand, one has to keep in mind that experimentally the 4 ML film is prepared by deposition of an additional layer on the ferromagnetic 3 ML film, so the system's transition to the thermal equilibrium state might be kinetically inhibited at room temperature. Indeed, it has been reported that in 4 ML films the ferromagnetic/paramagnetic transition at the Curie temperature ($\approx$333 K) is irreversible and coupled to a transition to a fairly undistorted fcc structure [96, 97].

4.2. The 5–10 ML coverage regime and the transition to bcc-Fe

With further deposition of iron, the complicated 5×1 reconstruction disappears and a $(2 \times 1)_{p2mg}$ phase develops, which is most pronounced at about 6 ML coverage and gradually disappears with further increasing film thickness. As already mentioned, in this coverage regime the Kerr signal is coverage independent. This is in line with the crystallographic structure obtained for the $(2 \times 1)_{p2mg}$ phase [64, 88, 89, 94]. As displayed in figure 8, the reconstruction of Fe layers is lifted, except for the top layer which exhibits antiparallel shifts of neighbouring atomic rows in the [011] direction according to the mirror plane evident in the LEED pattern. The interlayer spacings have relaxed to that of isotropic fcc, again except for the top layer whose spacing from the second layer is still expanded ($d_{12} = 1.87$ Å). This situation persists up to the range of 10–11 ML, though the $(2 \times 1)_{p2mg}$ phase seems to disappear. Yet, detailed LEED measurements and full dynamical quantitative analyses including that of diffuse intensities [88, 89] show that the antiparallel shifts of adjacent top-layer atomic rows are preserved locally, and only the long-range order of the reconstruction is lost. The mutual shift between atomic rows seems to vary only little with coverage ($2s_D = 0.3$–0.4 Å) and is in agreement with the expanded top-layer spacing, according to a hard-sphere model of

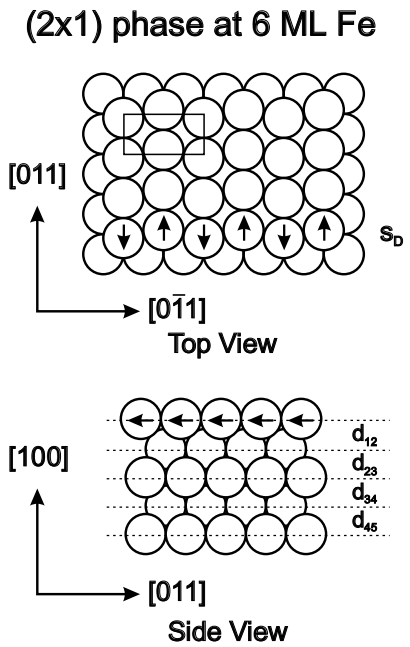

Figure 8. The structural model of the $(2 \times 1)_{p2mg}$ superstructure developing in the coverage range 5–10 ML Fe ($d_{12} = 1.87$ Å, $d_{23} = 1.78$ Å, $d_{34} = 1.76$ Å, $d_{45} = 1.77$ Å, $s_D \approx 0.2$ Å).

atoms. So, in the coverage regime from 5 up to 10–11 ML the film is almost completely and ideally fcc except for the top-layer spacing which still corresponds to a tetragonal distortion allowing for an increased atomic volume in the top two layers. Accordingly, only these layers couple ferromagnetically, so giving rise to the coverage-independent magnetic signal that is observed. The film region below seems to be non-magnetic or antiferromagnetic. First-principles calculations for a corresponding surface slab [51] produce a bilayer antiferromagnetic ground state for even numbers of Fe layers, whilst for odd numbers various spin structures coexist. In agreement with experiment, these films are isotropic fcc below the surface, yet only a small expansion ($\leqslant$1%) results for the top-layer spacing in contrast to the experimental finding ($\approx$5%). It has been argued that this is because the computations refer to zero temperature [51], yet we feel that the neglect of the surface reconstruction is a more probable source for the disagreement.

In the coverage range 10–11 ML the transition to bcc-iron develops, as quantitatively proved and determined again by LEED intensity analysis [85]. The precise critical coverage at which the transition to bcc takes place depends on many details of the preparation, e.g. on the iron deposition rate: lower rates lead to lower critical coverages. Also, residual (or intentional) gas adsorption has an influence and mild sputtering of the surface can trigger the transition [78]. In the transition range and slightly below and above, there is considerable disorder in the film, as indicated in the diffraction pattern by some background streaks and elongated spot shapes. With the transition completed, the (110) orientation of bcc-iron is parallel to the surface. As indicated in figure 9, the new phase differs from the former $(2 \times 1)_{p2mg}$ superstructure in the amount and direction of the shift of the atomic rows with respect to each other. In this respect, the $(2 \times 1)_{p2mg}$ phase can be understood as a precursor of the bcc(110) phase. One can imagine that on the top layer's in-plane shear proceeding to deeper layers, a coalescence of rows orthogonal to the shear direction takes place. This is accompanied by an increase of interlayer spacings and produces the configuration given schematically in the bottom panel of figure 9 ('pitch orientation' [79, 103]). Such a martensitic transformation has been observed in STM investigations [81, 82]. It is also obtained by LEED analyses in the transition range at 10–11 ML coverage. There, domains still having fcc structure and ones already transformed

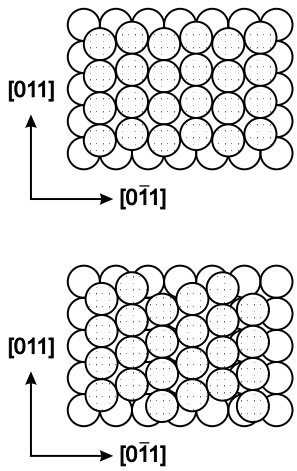

Figure 9. The $(2 \times 1)_{p2mg}$ phase (top) differs from the Fe(110) film (bottom) only in the amount and direction of shifts between adjacent [011] rows (apart from some small intra-row compression). Only the top layer of Fe atoms (hatched) is displayed in each case, for clarity.

to bcc structure have been found [85]. The bcc domains exhibit bcc(110) layers down to at least the fourth layer (according to the error limits), but most probably all layers of the film domain are bcc (in view of the minimum of the R-factor). The parallel existence of fcc and bcc domains (the latter grow at the expense of the former) indicates that the structural phase transition must be of first order. With completion of the transition, a practically ideal bcc-iron film is formed, with interlayer spacings identical within 0.03 Å to those of the (110) surface of an iron bulk crystal [85]. During the transition, the magnetization of the film changes (as displayed in figure 6) and eventually the magnetic anisotropy is parallel to the surface as in the case of a bulk iron crystal.

As already mentioned, the magnetic and structural properties of the ultrathin iron films depend considerably on the details of the film preparation. So, some of the above-described phases or growth regimes may not appear or may develop at different coverages. Also, whilst films deposited at room temperature (as described above) grow nearly layer by layer, those deposited at low temperatures (e.g. 130 K [91]) remain rather rough even after annealing. The presence of oxygen and carbon leads to some combined surfactant effect favouring rather smooth films and the incorporation of carbon within the iron lattice stabilizes fcc-iron up to very thick iron films [92, 93]. Also, it is reported that pulsed-laser-deposited ultrathin iron films on copper exhibit an isotropic fcc structure (reference [104]). Yet, the above-described reconstructions have also been found in laser-deposited films (reference [101]).

5. Conclusions

The three examples of ultrathin magnetic films grown epitaxially on non-magnetic substrates as presented above are rather different as regards the correlation between structural and magnetic properties. The case of Ni/Cu(100) is not very exciting from the crystallographic point of view, i.e. within the precision of surface structural tools such as quantitative LEED (here, of the order of 0.01 Å) no structural changes can be detected to accompany magnetic order–disorder transitions or spin reorientations. The slight tetragonal distortion observed is constant, homogeneous throughout the film and coverage independent. So, magnetostriction effects cannot be dramatically enhanced at the surface.

In contrast, the growth of cobalt films on Cu(111) exhibits—due to the different stacking sequences possible (fcc or hcp)—a variety of structural features related to the magnetic properties, in particular for Co/Cu superlattices. It appears that copper tends to float on top of the film surface in the case of very thin films. Then the stacking is fcc, obviously dictated and stabilized by the simultaneous presence of two Co–Cu interfaces. The floating process seems to be favoured by the deposition process itself, as the first cobalt double layer is incorporated into the substrate. With increasing film thickness the floating of copper is inhibited and hcp stacking develops rapidly. Yet, it can be converted back to fcc stacking by intentionally capping the film with copper layers, such as are present in Co/Cu superlattices. This is of importance for the magnetic properties of the latter, in particular their giant magnetoresistance, as stacking faults tend to reduce it.

The epitaxial system in which structural–magnetic correlations are most evident, diverse and complex is Fe/Cu(100). Though the lattice misfit is rather small, the films are not strictly pseudomorphic. In the low-coverage regime up to 4 ML, all iron layers are reconstructed with atomic movements both normal to the surface and in-plane, so the films are fcc on average at most. This is consistent with the ferromagnetism in the film, as according to first-principles calculations the accommodation of a high-atomic-spin state needs an increased atomic volume, which is indeed provided by the reconstruction. Of course, one cannot determine whether the magnetic state causes the reconstruction or vice versa—the features

are just consistent. Surprisingly, for thicker films (5–10 ML) the reconstruction of subsurface iron layers disappears and an isotropic fcc structure is formed. This indicates that the former reconstruction was not caused by epitaxial stress. With its disappearance in the subsurface region, the volume of the atoms involved decreases accordingly and—again consistently—the subsurface region becomes non-magnetic or antiferromagnetic. Only the top layer is still reconstructed, allowing for a high-atomic-spin state. At higher coverages a martensitic transition to bcc-iron takes place. We emphasize, however, that both the structural and magnetic properties seem to depend considerably on the details of the film preparation.

From the theoretical point of view, it seems that theory is able to reproduce the structural and magnetic properties of such comparably simple cases as Ni/Cu100) and possibly Co/Cu(111). However, the quantitative description of the system Fe/Cu(100) applies only to the gross features of this system. This seems to be due to the fact that explicit consideration of the complex geometrical reconstructions involved was not possible up to now. Fortunately, however, such work seems to be in progress.

Acknowledgments

The authors are indebted to the Deutsche Forschungsgemeinschaft (DFG) and Deutscher Akademischer Austauschdienst (DAAD) for several years of financial support. We also gratefully acknowledge long-standing collaborations with the groups of Professors K Baberschke (Berlin), H Ibach and M Wuttig (Jülich) and R Miranda (Madrid).

References

[1] Heinz K and Hammer L 1998 *Z. Kristallogr.* **213** 615
[2] Farle M 1998 *Rep. Prog. Phys.* **61** 755
[3] Stearns M B 1986 *Landolt–Börnstein New Series* Group III, vol 19, ed K-H Hellwege and O Madelung (Berlin: Springer)
[4] Schulz B and Baberschke K 1994 *Phys. Rev.* B **50** 13 467
[5] Müller S, Schulz B, Kostka G, Farle M, Heinz K and Baberschke K 1996 *Surf. Sci.* **364** 235
[6] Platow W, Bovensiepen U, Poulopoulos P, Farle M, Baberschke K, Hammer L, Walter S, Müller S and Heinz K 1999 *Phys. Rev.* B **59** 12 641
[7] Shen J, Giergiel J and Kirschner J 1995 *Phys. Rev.* B **52** 8454
[8] Heinz K 1988 *Prog. Surf. Sci.* **27** 239
[9] Heinz K 1995 *Rep. Prog. Phys.* **58** 695
[10] Pendry J B 1980 *J. Phys. C: Solid State Phys.* **13** 937
[11] Hjortstam O, Baberschke K, Wills J M, Johansson B and Eriksson O 1997 *Phys. Rev.* B **55** 15 026
[12] Cerdá J R, de Andres P L, Cebollada A, Miranda R, Navas E, Schuster P, Schneider C M and Kirschner J 1993 *J. Phys.: Condens. Matter* **5** 2055
[13] Le Dang K, Veillet P, Velu E, Parkin S S P and Chappert C 1993 *Appl. Phys. Lett.* **63** 108
[14] Kohlhepp J, Elmers H J and Gradmann U 1993 *J. Magn. Magn. Mater.* **121** 487
[15] Gonzalez L, Miranda R, Salmeron M, Verges J A and Yndurain F 1981 *Phys. Rev.* B **24** 3245
[16] Tonner B P, Han Z-L and Zhang J 1993 *Phys. Rev.* B **47** 9723
[17] Kief M T and Egelhoff W F Jr 1993 *Phys. Rev.* B **47** 10 785
[18] Camarero J, Spendeler L, Schmidt G, Heinz K, de Miguel J J and Miranda R 1994 *Phys. Rev. Lett.* **73** 2448
[19] de la Figuera J, Prieto J E, Kostka G, Müller S, Ocal C, Miranda R and Heinz K 1996 *Surf. Sci.* **349** L139
[20] Müller S, Kostka G, Schäfer T, de la Figuera J, Prieto J E, Ocal C, Miranda R, Heinz K and Müller K 1996 *Surf. Sci.* **352–354** 46
[21] Rath Ch, Prieto J E, Müller S, Miranda R and Heinz K 1997 *Phys. Rev.* B **55** 10 791
[22] Fauster Th, Rangelov G, Stober J and Eisenhut B 1993 *Phys. Rev.* B **48** 11 361
[23] Scheuch V, Potthast K, Voigtländer B and Bonzel H P 1994 *Surf. Sci.* **318** 115
[24] de la Figuera J, Prieto J E, Ocal C and Miranda R 1993 *Phys. Rev.* B **47** 13 043
[25] de la Figuera J, Prieto J E, Ocal C and Miranda R 1994 *Surf. Sci.* **307–309** 538

[26] de la Figuera J 1995 *Dissertation* Universidad Autónoma de Madrid
[27] Rabe A, Memmel N, Steltenpohl A and Fauster Th 1994 *Phys. Rev. Lett.* **73** 2728
[28] Hochstrasser M, Zurkirch M, Wetli E, Pescia D and Erbudak M 1994 *Phys. Rev. Lett.* **50** 17 705
[29] Le Fèvre P, Magnan H, Heckmann O, Briois V and Chandesris H 1995 *Phys. Rev.* B **52** 11 462
[30] Le Fèvre P, Magnan H and Chandesris H 1996 *Surf. Sci.* **352–354** 923
[31] Le Dang K, Veillet P, Hui He, Lamelas F J, Lee C H and Clarke R 1990 *Phys. Rev.* B **41** 12 902
[32] de Gronckel H A M, Kopinga K, de Jonge W J M, Panissod P, Schille J P and den Broeder F J A 1991 *Phys. Rev.* B **44** 9100
[33] Renard J P, Beauvillain P, Dupas C, Le Dang K, Veillet P, Velu E, Marliere C and Renard D 1992 *J. Magn. Magn. Matter* **115** L147
[34] Harp G R, Parkin S S P, Farrow R F C, Marks R F, Toney M F, Lam Q H, Rabedeau T A and Savoy R J 1993 *Phys. Rev.* B **47** 8721
[35] Lamelas F J, Lee C H, Hui He, Vavra W and Clarke R 1989 *Phys. Rev.* B **40** 5837
[36] Bödeker P, Abromeit A, Bröhl K, Sonntag P, Metoki N and Zabel H 1993 *Phys. Rev.* B **47** 2353
[37] Ascolani H, Cerdá J R, de Andres P L, de Miguel J J, Miranda R and Heinz K 1996 *Surf. Sci.* **345** 320
[38] Bruinsma R and Zangwill A 1985 *Phys. Rev. Lett.* **55** 214
[39] Redfield A C and Zangwill A M 1986 *Phys. Rev.* B **34** 1378
[40] Pedersen M O, Bönicke I A, Laegsgaard E, Stensgaard I, Ruban A, Norskov J K and Besenbacher F 1997 *Surf. Sci.* **387** 86
[41] Prieto J E, Rath Ch, Müller S, Miranda R and Heinz K 1998 *Surf. Sci.* **401** 248
[42] Marcus P M and Moruzzi V L 1988 *J. Appl. Phys.* **63** 4045
[43] Zhou G L, Yang M H and Flynn C P 1996 *Phys. Rev. Lett.* **77** 4580
[44] *NIST Surface Structure Data Base 3.0* 1999 National Institute of Standards and Technology, Gaithersburg, MD
[45] Jacobsen J, Nielsen L P, Besenbacher F, Stensgaard I, Laegsgaard E, Rasmussen T, Jacobsen W and Norskov J K 1995 *Phys. Rev. Lett.* **75** 489
[46] Moruzzi V L, Marcus P M, Schwarz K and Mohn P 1986 *Phys. Rev.* B **34** 1784
[47] Moruzzi V L, Marcus P M and Kübler J 1989 *Phys. Rev.* B **39** 6957
[48] Weiss R J 1963 *Proc. R. Soc.* **82** 281
[49] Kraft T, Marcus P M and Scheffler M J 1994 *Phys. Rev.* B **49** 11 511
[50] Asada T and Blügel S 1997 *Phys. Rev. Lett.* **79** 507
[51] Moroni E G, Kresse G and Hafner J 1999 *J. Phys.: Condens. Matter* **11** L35
[52] Hallbauer R and Gonser A 1983 *J. Magn. Magn. Mater.* **35** 55
[53] Onellion M, Thompson M A, Erskine J L, Duke C B and Paton A 1987 *Surf. Sci.* **179** 219
[54] Darici Y, Marcano J, Min H and Montano P A 1987 *Surf. Sci.* **182** 477
[55] Clarke A, Rous P J, Arnott M, Jennings G and Willis R F 1987 *Surf. Sci.* **192** L843
[56] Chambers S A, Wagener T J and Weaver J H 1987 *Phys. Rev.* B **36** 8992
[57] Steigerwald D A and Egelhoff W F Jr 1987 *Surf. Sci.* **192** L887
[58] Macedo W A and Keune W 1988 *Phys. Rev. Lett.* **61** 475
[59] Steigerwald D A, Jacob I and Egelhoff W R Jr 1988 *Surf. Sci.* **202** 472
[60] Daum W, Stuhlmann C and Ibach H 1988 *Phys. Rev. Lett.* **60** 2741
[61] Lu S H, Quinn J, Tian D, Jona F and Marcus P M 1989 *Surf. Sci.* **209** 364
[62] Darici Y, Marcano J, Min H and Montano P A 1989 *Surf. Sci.* **217** 521
[63] Egawa C, McCash E M and Willis R F 1989 *Surf. Sci.* **215** L271
[64] Landskron H, Schmidt G, Heinz K, Müller K, Stuhlmann C, Beckers U, Wuttig M and Ibach H 1991 *Surf. Sci.* **256** 115
[65] Glatzel H, Fauster T, Scherzer B M U and Dose V 1991 *Surf. Sci.* **254** 58
[66] Magnan H, Chandesris D, Villette B, Heckmann O and Lecante J 1991 *Phys. Rev. Lett.* **67** 859
[67] Arnott M, McCash E M and Allison W 1992 *Surf. Sci.* **269+270** 724
[68] Xhonneux P and Courtens E 1994 *Phys. Rev.* B **46** 5567
[69] Thomassen J, May F, Feldmann B, Wuttig M and Ibach H 1992 *Phys. Rev. Lett.* **69** 3831
[70] Pappas D P, Brundle C R and Hopster H 1992 *Phys. Rev.* B **45** 8169
[71] Allenspach R and Bischof A 1992 *Phys. Rev. Lett.* **69** 3385
[72] Thomassen J, Feldmann B and Wuttig M 1992 *Surf. Sci.* **264** 406
[73] Wuttig M and Thomassen J 1993 *Surf. Sci.* **282** 273
[74] Brodde A and Neddermeyer H 1993 *Surf. Sci.* **287+288** 988
[75] Johnson K E, Chambliss D D, Wilson R J and Chiang S 1993 *J. Vac. Sci. Technol.* A **11** 1654
[76] Detzel T, Memmel N and Fauster T 1993 *Surf. Sci.* **293** 227
[77] Bayer P, Müller S, Schmailzl P and Heinz K 1993 *Phys. Rev.* B **48** 17 611

[78] Wuttig M, Feldmann B, Thomassen J, May F, Zillgen H, Brodde A, Hennemann H and Neddermeyer H 1993 *Surf. Sci.* **291** 14
[79] Scheuer F, Allenspach R, Xhonneux P and Courtens E 1993 *Phys. Rev.* B **48** 9890
[80] Nyberg G L, Kief M T and Egelhoff W F Jr 1993 *Phys. Rev.* B **48** 14 509
[81] Kalki K, Chambliss D D, Johnson K E, Wilson R J and Chiang S 1993 *Phys. Rev.* B **48** 18 344
[82] Giergiel J, Kirschner J, Landgraf J, Shen J and Woltersdorf J 1994 *Surf. Sci.* **310** 1
[83] Li D, Freitag M, Pearson J, Qiu Z Q and Bader S D 1994 *Phys. Rev. Lett.* **72** 3112
[84] Memmel N and Detzel T 1994 *Surf. Sci.* **307–309** 490
[85] Schmailzl P, Schmidt K, Bayer P, Döll R and Heinz K 1994 *Surf. Sci.* **312** 73
[86] Müller S, Bayer P, Reischl C, Heinz K, Feldmann B, Zillgen H and Wuttig M 1995 *Phys. Rev. Lett.* **74** 765
[87] Heinz K, Müller S and Bayer P 1995 *Surf. Sci.* **337** 215
[88] Heinz K, Bayer P and Müller S 1995 *Surf. Rev. Lett.* **2** 89
[89] Müller S, Bayer P, Kinne A, Schmailzl P and Heinz K 1995 *Surf. Sci.* **322** 21
[90] Müller S, Bayer P, Kinne A, Reischl C, Metzler R and Heinz K 1995 *Surf. Sci.* **331–333** 723
[91] Giergiel J, Shen J, Woltersdorf J, Kirilyuk A and Kirschner J 1995 *Phys. Rev.* B **52** 8528
[92] Kirilyuk A, Giergiel J, Shen J and Kirschner J 1995 *Phys. Rev.* B **52** R11 672
[93] Kirilyuk A, Giergiel J, Shen J, Straub M and Kirschner J 1996 *Phys. Rev.* B **54** 1050
[94] Heinz K, Müller S and Bayer P 1996 *Surf. Sci.* **352–354** 942
[95] Straub M, Vollmer R and Kirschner J 1996 *Phys. Rev. Lett.* **77** 743
[96] Zharnikov M, Dittschar A, Kuch W, Schneider C M and Kirschner J 1996 *Phys. Rev. Lett.* **76** 314
[97] Zharnikov M, Dittschar A, Kuch W, Schneider C M and Kirschner J 1997 *J. Magn. Magn. Mater.* **174** 40
[98] Berger A, Feldmann B, Zillgen H and Wuttig M 1998 *J. Magn. Magn. Mater.* **183** 35
[99] Shen J, Mohan Ch V, Ohresser P, Klaua M and Kirschner J 1998 *Phys. Rev.* B **57** 13 674
[100] Shen J, Jenniches H, Mohan Ch V, Barthel J, Klaua M, Ohresser P and Kirschner J 1998 *Europhys. Lett.* **43** 349
[101] Weinelt M, Schwarz S, Baier H, Müller S, Hammer L, Heinz K and Fauster Th 1999 to be published
[102] Döll R, Kottcke M and Heinz K 1993 *Phys. Rev.* B **48** 1973
[103] Pitsch W 1959 *Phil. Mag.* **4** 577
[104] Jenniches H, Shen J, Mohan Ch V, Manoharan Mohan S, Barthel J, Ohresser P, Klaua M and Kirschner J 1999 *Phys. Rev.* B **59** 1196